We are IntechOpen, the world's leading publisher of Open Access books
Built by scientists, for scientists

6,900
Open access books available

185,000
International authors and editors

200M
Downloads

154
Countries delivered to

Our authors are among the

TOP 1%
most cited scientists

12.2%
Contributors from top 500 universities

CLARIVATE ANALYTICS
BOOK CITATION INDEX
INDEXED

WEB OF SCIENCE™

Selection of our books indexed in the Book Citation Index
in Web of Science™ Core Collection (BKCI)

Interested in publishing with us?
Contact book.department@intechopen.com

Numbers displayed above are based on latest data collected.
For more information visit www.intechopen.com

Potential-pH Diagrams for Oxidation-State Control of Nanoparticles Synthesized via Chemical Reduction

Shunsuke Yagi
Nanoscience and Nanotechnology Research Center,
Osaka Prefecture University
Japan

1. Introduction

In the past, many synthesis methods of nanoparticles have been reported, but the synthesis processes have not been well discussed from the viewpoint of thermodynamics. In this chapter, a general concept using potential-pH diagrams is described for oxidation-state control of nanoparticles synthesized via chemical reduction (also called electroless deposition or liquid-phase reduction). By comparing kinetically determined mixed potential measured in reaction solution and thermodynamically drawn potential diagrams, e.g., potential–pH diagram, it is possible to know "what chemical species is stable in the reaction solution?." It is predicted from potential-pH diagrams that nanoparticles in different oxidation states can be selectively synthesized by controlling the mixed potential. This concept is verified by selectively synthesizing Cu and Cu_2O nanoparticles from CuO aqueous suspension via chemical reduction using the concept as an example. The advantage of this chemical reduction method is that abundant nanoparticles can be obtained for a short time by a simple operation. An extremely small activity of Cu^{2+} aquo ion is achieved by using insoluble CuO powder as a Cu(II) ionic source, which is a key for the synthesis of nanosized particles. The dependency of mixed potential on pH and temperature is discussed in the verification process. This chapter is written based on the result of the authors' paper (Yagi et al., 2009) with further detailed information on practical thermodynamic calculation and drawing procedure of potential-pH diagrams.

2. Brief overview of objective materials and their synthesis

2.1 Copper (Cu) nanoparticles

Copper (Cu) nanoparticles are of great interest in various fields, specifically that of printable electronics. Cu interconnects less than 20 µm wide can be made with a high resolution screen printer or a super inkjet printer using an ink which contains dense Cu nanoparticles. Cu nanoparticles have been synthesized by various reduction processes from cuprous (Cu(I)) or cupric (Cu(II)) compounds, including direct electrochemical reduction (Han et al., 2006; L. Huang et al., 2006; Yu et al., 2007), chemical reduction (Lisiecki & Pileni, 1993; Lisiecki et al., 1996; H. H. Huang et al., 1997; Qi et al., 1997; Ohde et al., 2001), thermal reduction (Dhas et al.,

1998), sonochemical reduction (Dhas et al., 1998; Kumar et al., 2001), laser irradiation (Yeh et al., 1999), and gamma radiolysis (Joshi et al., 1998). Many of these methods are conducted in liquid phase, which has the important advantage that nanoparticles can be formed in the presence of dispersing agents and no additional process for the addition of dispersing agents is required for the fabrication of inks to avoid the agglomeration.

In recent years, Cu nanoparticle also has drawn a lot of attention due to its novel optical properties from surface plasmon resonance (SPR), which occurs when a light electromagnetic field drives the collective oscillation of free electrons in Cu nanoparticles (J. Li et al., 2011). This resonance creates large local electric field enhancement on the nanoparticle surface, which can be used to manipulate light–matter interactions and boost non-linear phenomena. The SPR of Cu nanoparticles is observed at 560-580 nm, which is slightly changed by a medium and a dispersing/protecting agent (Singh et al., 2010; X.D. Zhang et al., 2011), and Pileni and Lisiecki demonstrated the strong broadening of the plasmon peak for Cu nanoparticles with decreasing the particle size (Pileni & Lisiecki, 1993). In addition, Cu nanoparticles display fluorescence. Siwach and Sen reported fluorescence peaks at ca. 296 nm for excitation wavelength at 213 nm and 270 nm using Cu nanoparticles about 13 nm in diameter in water (Siwach & Sen, 2010).

2.2 Cuprous oxide (Cu₂O) nanoparticles

Cuprous oxide (Cu_2O) is a p-type semiconductor (Young & Schwartz, 1969) with unique optical and magnetic properties (Mahajan et al., 2009) and is also a promising material with potential applications in solar energy conversion, microelectronics, magnetic storage, catalysis, photocatalysis (Gu et al., 2010), and gas sensing (Zhang et al., 2006). Cu_2O is also used for the investigation into Bose–Einstein condensation of excitons (Snoke, 2002). Many methods have been reported to synthesize Cu_2O nanoparticles (Zhang et al., 2006; Muramatsu & Sugimoto, 1997; X. Liu et al., 2007), nanocubes (Gou & Murphy, 2003; R. Liu et al., 2003), octahedral nanocages (Lu et al., 2005), nanorods (Cheng et al., 2011), and nanowires (Wang et al, 2002). For example, Muramatsu and Sugimoto reported that Cu_2O particles with an average diameter of 270 nm were synthesized in large quantities from a CuO aqueous suspension using hydrazine as the reducing agent (Muramatsu & Sugimoto, 1997). Liu et al. formed CuO, Cu_2O, and Cu nanoparticles using copper(II) acetylacetonate [$Cu(acac)_2$] as a precursor in oleylamine by controlling temperature (Liu et al., 2007).

It is noteworthy that nanoparticles of transition-metal oxides including Cu_2O and CuO are also expected as a negative electrode material with a high specific capacity and extraordinary large surface area for lithium ion battery (Poizot et al., 2000). The cycle property of Cu_2O nanoparticles is strongly dependent on the particle size, shape, and structure; there is an optimum condition, displaying the highest electrochemical performance (C.Q. Zhang et al., 2007).

In the next section, a general guideline is introduced for the selective synthesis of Cu and Cu_2O nanoparticles possessing superior properties described above from the same CuO aqueous suspension.

3. Theory for oxidation-state control of nanoparticles

3.1 Mixed potential

At any point within the reaction volume during nanoparticle synthesis via chemical reduction, several partial reactions occur in parallel (e.g. oxidation of a reducing agent,

reduction of metallic ion, reduction of dissolved oxygen, and solvent reduction decomposition). The potential at a point is determined at the value where the total of anodic currents $I_{a,total}$ (currents for oxidation reaction) balances the total of cathodic currents $I_{c,total}$ (currents for oxidation reaction) unless current flows outside (Fig. 1). This potential is called the mixed potential. Stable chemical species in the reaction solution can be determined by comparing measured mixed potential and calculated potential diagrams, and chemical species synthesized can be changed by controlling mixed potential. As an example, considering a reaction system for the synthesis of Cu or Cu_2O nanoparticles from a CuO aqueous "suspension" of pH 9 via hydrazine reduction, anodic reactions are mainly the oxidation reactions of hydrazine as follows

$$N_2H_4 + 4OH^- \rightarrow N_2 + 4H_2O + 4e \tag{1}$$

$$N_2H_4 + OH^- \rightarrow 1/2N_2 + NH_3 + H_2O + e \tag{2}$$
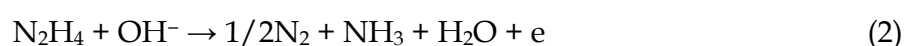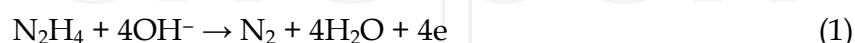
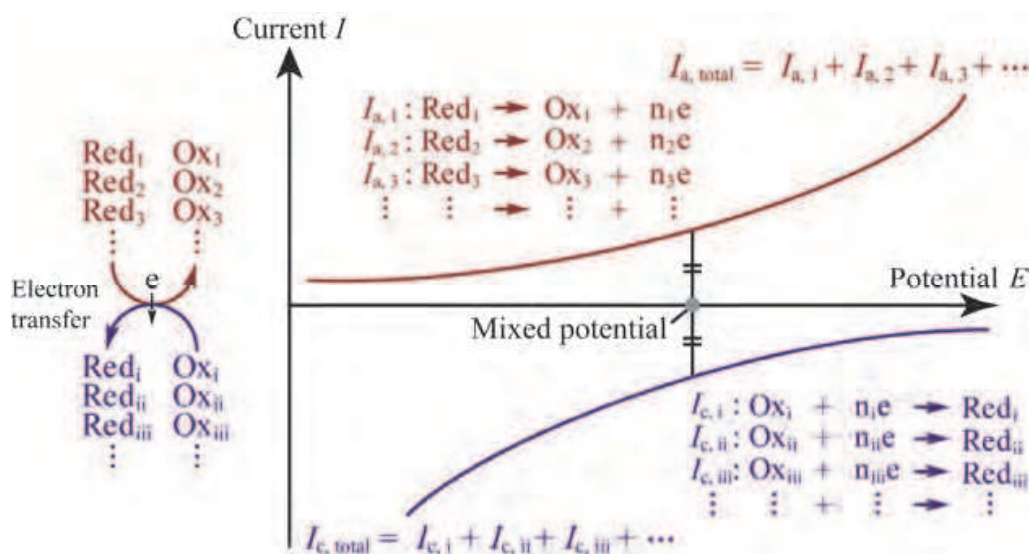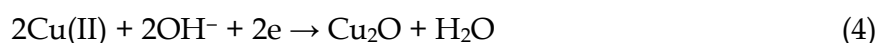Cathodic reactions are mainly the deposition of Cu or Cu_2O and hydrogen generation as follows

Fig. 1. Schematic current-potential curves: mixed potential is determined at the value where the total of anodic currents $I_{a,total}$, balances the total of cathodic currents $I_{c,total}$, unless current flows outside.

Deposition of Cu

$$Cu(II) + 2e \rightarrow Cu \tag{3}$$
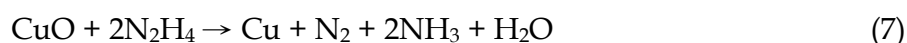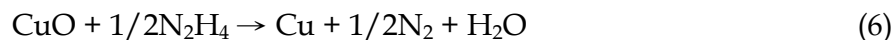
Deposition of Cu_2O

$$2Cu(II) + 2OH^- + 2e \rightarrow Cu_2O + H_2O \tag{4}$$

Hydrogen generation

$$2H_2O + 2e \rightarrow H_2 + 2OH^- \tag{5}$$

where Cu(II) represents all the copper(II) species and is distinguished from a copper(II) aquo ion, Cu^{2+}. The overall deposition reactions of Cu and Cu_2O in this system can be expressed using the following equations

Deposition of copper

$$CuO + 1/2N_2H_4 \rightarrow Cu + 1/2N_2 + H_2O \tag{6}$$

$$CuO + 2N_2H_4 \rightarrow Cu + N_2 + 2NH_3 + H_2O \tag{7}$$

Deposition of cuprous oxide

$$2CuO + 1/2N_2H_4 \rightarrow Cu_2O + 1/2N_2 + H_2O \tag{8}$$

$$2CuO + 2N_2H_4 \rightarrow Cu_2O + N_2 + 2NH_3 + H_2O \tag{9}$$

In practice, the "absolute" mixed potential cannot be measured because of the following experimental reason (Bockris et al., 2000). When one tries to measure the mixed potential using potentiometers, two metallic terminals of the potentiometers must be connected to the two electrodes immersed in the reaction solution (electrolyte). In this case, all one can measure is the potential "difference" across the two electrode/electrolyte interfaces. Each electrode/electrolyte interface has a potential difference due to a double layer between the electrode and electrolyte, and thus, the measured potential difference includes at least two potential differences at different interfaces. In other words, when one tries to measure one potential difference, one must create at least one additional potential difference. This is not favorable, but inevitable. However, by using a nonpolarizable electrode as one electrode, the measured potential difference directly reflects the change in the potential difference of the other electrode/electrolyte interface because the potential difference of the nonpolarizable electrode/electrolyte interface does not change. Therefore, the measured potential difference can be treated as the "relative" mixed potential by using a nonpolarizable electrode as a reference electrode, e.g. standard hydrogen electrode, Ag/AgCl electrode, and saturated calomel electrode. In addition, the other measuring electrode should not have a strong catalytic activity for possible reactions in order not to affect the original balance of anodic currents and cathodic currents so much, which can cause the change in the mixed potential. In the present system, a gold electrode is appropriate as a measuring electrode since gold has a low catalytic activity for hydrazine decomposition or hydrogen generation.

3.2 Potential-pH diagram (Pourbaix diagram)

Potential-pH diagram is a kind of phase diagram showing possible stable phases of an electrochemical system in equilibrium. Potential-pH diagram was invented by Marcel Pourbaix (1904-1998) and is also known as Pourbaix diagram (Pourbaix, 1966). In the potential-pH diagram, the vertical axis is potential normally with respect to the standard hydrogen electrode (SHE) and the horizontal axis is pH($=-\log a_{H+}$), where a_{H+} is the activity of proton. By comparing the potential-pH diagram and the mixed potential described above, it is possible to know the stable or obtainable chemical species in the reaction solution.

3.3 How to draw potential-pH diagram

In order to draw potential-pH diagram, it is necessary to determine the activity of ionic species. For example, consider an equilibrium reaction of metallic oxide M_xO_y and M^{z+} aquo ion in an aqueous solution as follows;

$$M_xO_y + 2yH^+ = xM^{z+} + yH_2O \tag{10}$$

where M is a metal and M^{z+} is a metallic aquo ion. There is a relationship $2y=xz$, which is derived from the charge balance of the reaction 10. The following equation indicates the change in Gibbs free energy, ΔG_T of the reaction 10 at absolute temperature T in kelvins and 1 atm.

$$\Delta G_T = \Delta G_T^0 + RT \ln \frac{a_{M^{z+}}^x a_{H_2O}^y}{a_{M_xO_y} a_{H^+}^{2y}} \tag{11}$$

where ΔG_T^0 is the change in Gibbs free energy at a standard state and a temperature T (K), and R is the gas constant. In equilibrium, the change in Gibbs free energy is zero and thus

$$0 = \Delta G_T^0 + RT \ln \frac{a_{M^{z+}}^x a_{H_2O}^y}{a_{M_xO_y} a_{H^+}^{2y}} \tag{12}$$

ΔG_T^0 can be calculated by the following equation using thermodynamic data;

$$\Delta G_T^0 = \Delta H_T^0 - T\Delta S_T^0 = \Delta H_{298}^0 + \int_{298}^T \Delta C_P dT - T\left(\Delta S_{298}^0 + \int_{298}^T \frac{\Delta C_P}{T} dT\right) \tag{13}$$

where ΔH_T^0 and ΔS_T^0 are the changes in enthalpy and entropy that accompanies the formation of 1 mole of a product from its component elements at a temperature T (K) and 1 atm. ΔC_p is the change in specific heat at constant pressure (1 atm). The absolute value of enthalpy H cannot be measured but chemical reaction system is a closed reaction system, and the change in enthalpy can be obtained by just subtracting the sum of the heat of formation, which is measurable, of the components in the left-hand side from that of the components in the right-hand side. Thermodynamic databooks include the list of the standard heat of formation, standard entropy at 298 K, and specific heat (Kubaschewski & Alcock, 1979; Latimer 1959; Stull & Prophet, 1971). Going back to the equation 12, the activities of water and oxide are both 1, and the equation 12 is simplified into the relationship between pH and the activity of the metallic aquo ion.

$$2y\text{pH} = -\frac{\Delta G_T^0}{\ln(10)RT} - x \log a_{M^{z+}} \tag{14}$$

Thus, the pH value, at which M_xO_y and M^{z+} are in equilibrium, is determined by the activity of the metallic aquo ion. Conversely, the activity of the metallic aquo ion in equilibrium can be determined by measured or maintained pH of a metallic oxide reaction suspension.

In the present system, CuO powder is dispersed in the reaction solution. When the pH of the reaction solution is 9 and the temperature is 298 K, the activity of Cu^{2+} aquo ion is calculated to be about 7.5×10^{-11} using the thermodynamic data shown in Table 1 (Criss & Cobble, 1964; Kubaschewski & Alcock, 1979; Latimer 1959; Stull & Prophet, 1971). This value itself does not have a precise meaning; the calculated value of the activity of Cu^{2+} aquo ion can be significantly affected by an experimental error of thermodynamic data, e.g. the standard entropy of CuO. Normally, this value just indicates that CuO does not dissolve into the solution in a practical sense. However using this value, one can calculate other important thermodynamic values such as the oxidation-reduction (redox) potential of Cu^{2+}/Cu redox pair in this reaction system using the same thermodynamic data set.

Chemical species	Standard heat of formation (kJ mol⁻¹)	Standard entropy (J K⁻¹ mol⁻¹)	Specific heat at constant pressure (J K⁻¹ mol⁻¹) $C_p = a + bx10^{-3}T + cx10^5T^2$		
$H^+(aq)$	0.0	0.0	129.7	–	–
$Cu^{2+}(aq)$	64.4	−98.7	267.8	–	–
$H_2O(l)$	−285.8	70.0	75.4	–	–
$H_2(g)$	0.0	130.6	27.3	3.3	0.50
$Cu(s)$	0.0	33.1	22.6	6.3	–
$Cu_2O(s)$	−167.4	93.1	62.3	23.9	–
$CuO(s)$	−155.2	42.7	38.8	20.1	–
$N_2(g)$	0.0	191.5	27.9	4.3	–
$NH_3(g)$	−45.9	192.7	37.3	18.7	−6.49
$N_2H_4(l)$	50.6	121.6	72.7	87.2	0.60

Table 1. List of standard heat of formation, entropy at 298 K and 1 atm, and specific heat at constant pressure (1 atm) considered and used for thermodynamic calculation. The units of the original data are converted to match the SI units using the thermochemical calorie, 1 cal$_{th}$=4.184 J. All the data considered and used for thermodynamic calculation are listed in this table. Only the constant a and coefficients b and c for the specific-heat capacity of hydrazine are estimated by fitting the discrete data of the specific heat capacity of hydrazine in the temperature range from 100 to 600 K. The data of liquid hydrazine $N_2H_4(l)$, are used instead of those of hydrated hydrazine $N_2H_4(aq)$, because of the lack of the data of $N_2H_4(aq)$.

The procedure to draw potential–pH diagram is shown in Fig. 2. In this system, the equilibrium pH between Cu^{2+} aquo ion with the activity of 7.5 x 10⁻¹¹ and CuO is 9, which is obvious and can also be checked by substituting the activity of Cu^{2+} ions into the equation 14. This equilibrium relationship can be represented by the vertical line 1 (Fig. 2a). The equilibrium activity of Cu^{2+} ions exceeds the determined value (7.5 x 10⁻¹¹) in the left region of the line 1 and underruns it in the right region. On the other hand, the redox potential of Cu^{2+}/Cu redox pair with respect to the standard hydrogen electrode can be determined by considering the electromotive force between the following half-cell reactions:
Copper deposition

$$Cu^{2+} + 2e = Cu \qquad (15)$$

Hydrogen generation at a standard state (the activities of proton and hydrogen gas are both 1)

$$2H^+ + 2e = H_2 \qquad (16)$$

The total cell reaction is obtained by subtracting the equation 16 from the equation 15 to erase the electron term.

$$Cu^{2+} + H_2 = Cu + 2H^+ \qquad (17)$$

Potential-pH Diagrams for
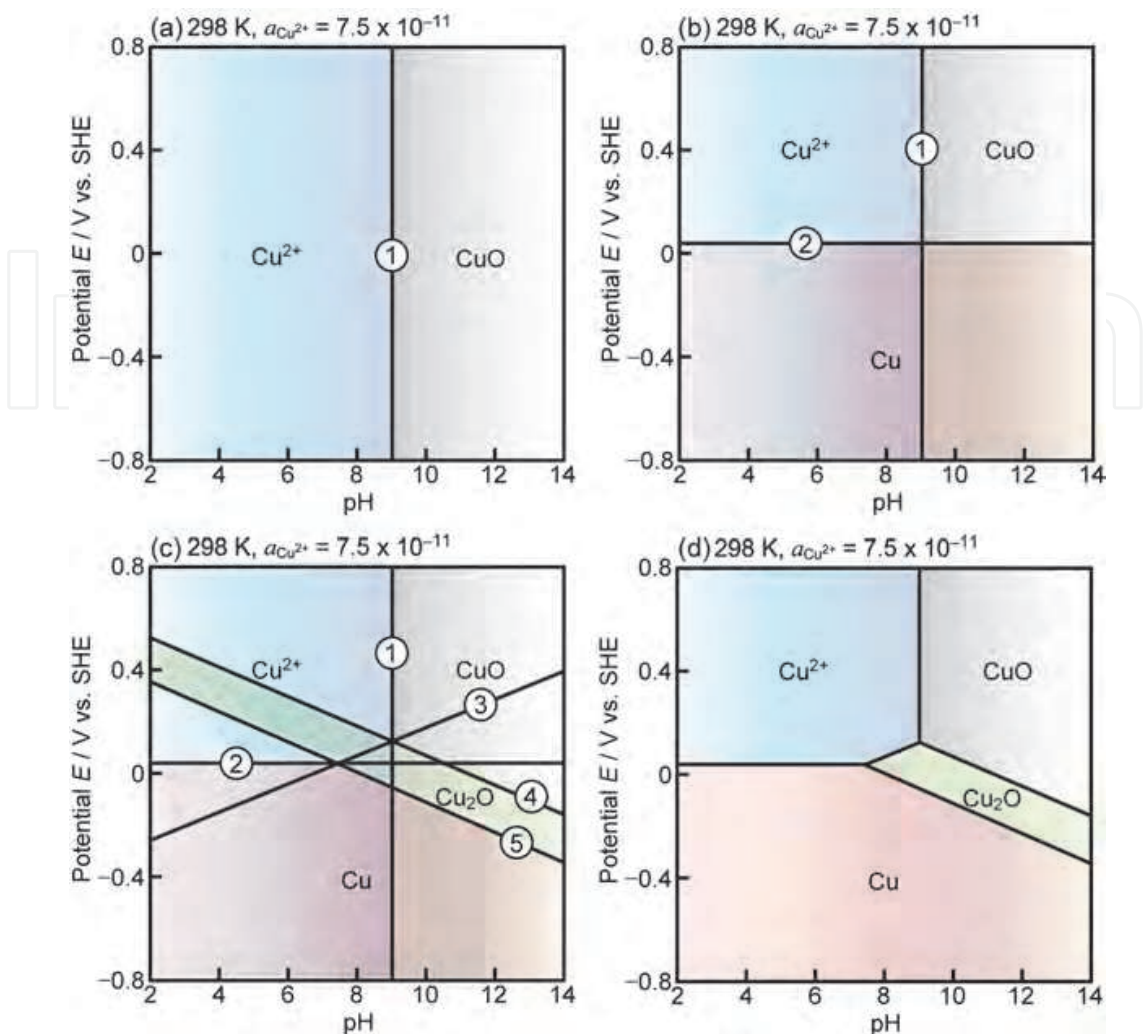Oxidation-State Control of Nanoparticles Synthesized via Chemical Reduction
229

Fig. 2. Procedure to draw potential–pH diagram at pH 9 and 298 K in a CuO aqueous suspension. Vertical line indicates the equilibrium relationship of an acid-base reaction and horizontal line indicates that of a redox reaction. Diagonal line indicates an equilibrium relationship of the reaction including both an acid-base reaction and a redox reaction. In this procedure, the equilibrium activities of Cu^{2+} aquo ion was set to be 7.5×10^{-11} considering the following copper species; Cu^{2+}, CuO, Cu_2O, and Cu. Oxyanions of copper, $HCuO_2^-$ and CuO_2^{2-}, or hydroxyanions of copper, $Cu(OH)_3^-$ and $Cu(OH)_4^{2-}$ (Beverskog, 1997), are not considered for simplicity. In order to include such ions, one should consider all the additional possible equilibrium relationships.

The redox potential E_T at a temperature T and 1 atm of Cu^{2+}/Cu redox pair is calculated using the following Nernst equation

$$
\begin{aligned}
E_T &= -\frac{\Delta G_T}{nF} = -\frac{1}{nF}\left(\Delta G_T^0 + RT\ln Q\right) \\
&= -\frac{1}{nF}\left[\left(\Delta H_T^0 - T\Delta S_T^0\right) + RT\ln Q\right] \\
&= -\frac{1}{nF}\left[\left(\Delta H_{298}^0 + \int_{298}^T \Delta C_P dT\right) - T\left(\Delta S_{298}^0 + \int_{298}^T \frac{\Delta C_P}{T}dT\right) + RT\ln Q\right]
\end{aligned}
\tag{18}
$$

where, n is the number of electrons transferred in the reaction, F is the Faraday constant. Q is the reaction quotient, which is expressed as the following equation 19 for the calculation of the redox potential of Cu^{2+}/Cu redox pair considering that the activities of metallic copper, proton and hydrogen gas in the standard hydrogen electrode are all 1:

$$Q = \frac{a_{Cu}a_{H^+}^2}{a_{Cu^{2+}}a_{H_2}} = \frac{1}{a_{Cu^{2+}}} \tag{19}$$

It should be noted that ΔG_T is the "total" Gibbs free energy change, including hydrogen oxidation as in the total cell equation 17. When CuO and Cu^{2+} ions are in equilibrium at pH 9 (the activity of Cu^{2+} ions is 7.5 x 10^{-11}), the redox potential is calculated to be 0.036 V vs. SHE using the equation 18. This equilibrium relationship is represented by the horizontal line 2 (Fig. 2b). The region above the line is the stability region of Cu^{2+} ions (with a higher oxidation number +II) and the region below the line is the stability region of Cu (with a lower oxidation number 0).

Equation 10 is a simple acid-base reaction (proton exchange reaction), and a unique equilibrium pH is determined. Similarly, equation 15 is a simple redox reaction (electron exchange reaction), and a unique equilibrium potential is determined. There is also a combination reaction of an acid-base reaction and a redox reaction (proton and electron exchange reaction). In this case, the equilibrium relationship is expressed also by Nernst equation (equation 18), which provides a relational expression between potential E_T and pH. In the present system, equilibrium relationships of Cu^{2+}/Cu_2O, CuO/Cu_2O, and Cu_2O/Cu are all categorized as this kind of reaction (proton and electron exchange reaction), corresponding to the diagonal lines 3, 4, and 5 in Fig. 2c, respectively.

After all of the possible equilibrium lines are drawn in the diagram, a part of the equilibrium lines are deleted to leave the common stability regions. Figure 2d is a potential-pH diagram drawn by the above procedure. As can be seen from this procedure, potential-pH diagram can be altered by a set of chemical species and conditions considered, e.g. temperature, activity of ions. Therefore, the selection of chemical species in addition to the activity settings is important and should be done according to an intended purpose: for example, dissolution of chemicals, corrosion proof, electrolysis, and electroless deposition.

3.4 Potential-pH diagrams for Cu and Cu_2O nanoparticles formation system

Figure 3 shows potential–pH diagrams drawn at an equilibrium activity of the Cu^{2+} aquo ion in the presence of abundant CuO at pH 9 in accordance with the procedure written in the section 3.3. The equilibrium activity of Cu^{2+} aquo ion is determined by considering an equilibrium reaction of Cu^{2+} and CuO, where the activities of CuO and H^+ are assigned to 1 and 10^{-9}, respectively. The species Cu^{2+}, CuO, Cu_2O, and Cu are only considered, and oxyanions of copper, such as $HCuO_2^-$ and CuO_2^{2-}, or hydroxyanions of copper, $Cu(OH)_3^-$ and $Cu(OH)_4^{2-}$, are not considered. This is only for simplicity because the redox potentials of CuO/Cu_2O and Cu_2O/Cu redox pairs at pH 9 are important for the prediction of synthesized chemical species in the present system. For instance, the redox potentials of Cu_2O and any Cu(II) ionic species in equilibrium are the same at a constant pressure, pH, and temperature in the presence of abundant solid CuO powder, resulting in the same redox potential of the Cu_2O/Cu redox pair. The equilibrium activity of Cu^{2+} aquo ion changes with pH and therefore, the potential–pH diagram is only valid at the constant pH considered. Fortunately, pH of the solution barely changes during the reaction in the

Potential-pH Diagrams for
Oxidation-State Control of Nanoparticles Synthesized via Chemical Reduction
231

present case, and it is possible to determine the most stable chemical species throughout the reaction by comparing the measured mixed potential to the vertical line of a constant pH (in this case, pH 9) in the potential–pH diagrams. In other words, the kind of chemical species synthesized can be controlled if the mixed potential is changed as expected.
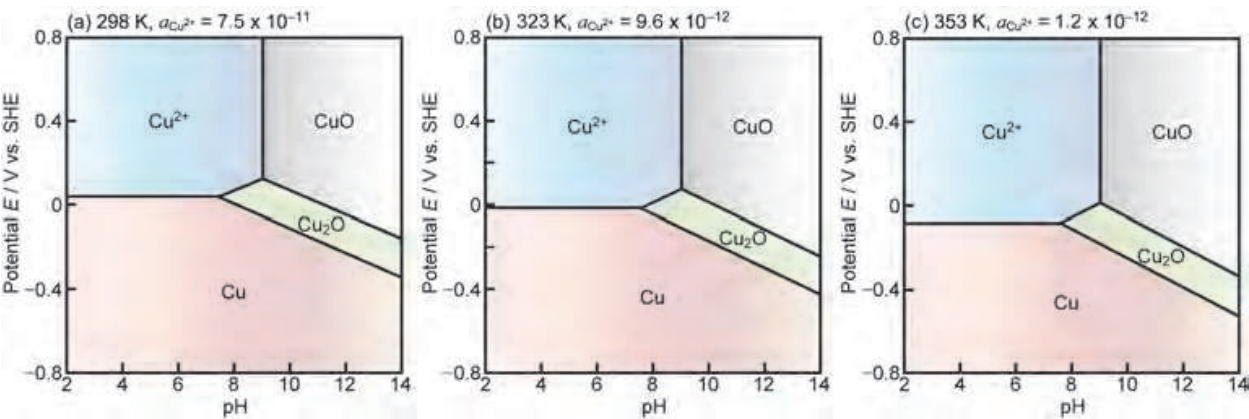

Fig. 3. Potential–pH diagrams drawn at the equilibrium activities of Cu^{2+} aquo ion at pH 9 and (a) 298, (b) 323, and (c) 353 K considering the species Cu^{2+}, CuO, Cu_2O, and Cu. Oxyanions of copper, $HCuO_2^-$ and CuO_2^{2-}, or hydroxyanions of copper, $Cu(OH)_3^-$ and $Cu(OH)_4^{2-}$, are not considered for simplicity. These potential–pH diagrams are only valid at the vertical line of pH 9 because the equilibrium activity of Cu^{2+} aquo ion changes with pH in this system.

Partial reaction	Redox potential at pH 9 (V vs. SHE)			Redox potential at pH 12 (V vs. SHE)			Reaction no.
	298 K	323 K	353 K	298 K	323 K	353 K	
$N_2 + 4H_2O + 4e = N_2H_4 + 4OH^-$	−0.92	−0.98	−1.06	−1.09	−1.17	−1.27	(1)
$1/2N_2 + NH_3 + H_2O + e = N_2H_4 + OH^-$	−2.59	−2.72	−2.88	−2.77	−2.91	−3.09	(2)
$Cu(II) + 2e = Cu$	0.04	−0.02	−0.08	−0.14	−0.21	−0.29	(3)
$2Cu(II) + 2OH^- + 2e = Cu_2O + H_2O$	0.13	0.07	0.01	−0.05	−0.12	−0.20	(4)
$2H_2O + 2e = H_2 + 2OH^-$	−0.18	−0.19	−0.21	−0.35	−0.38	−0.42	(5)

Table 2. List of redox potentials calculated for partial reactions considered in this system. Activity of each chemical species is substituted by the actual molar concentration in the present reaction system, and specifically, activities of H_2 and NH_3 are both substituted by 10^{-6} to obtain reference values.

3.5 How to control the mixed potential?

As described in the section 3.1, the mixed potential is determined by the balance of each partial current. Therefore, the mixed potential is altered when the redox potential of each partial reaction is changed. The redox potential E_T at a temperature T and 1 atm is calculated using the Nernst equation (equation 18). Table 2 shows calculated results of the redox potentials of all the partial reactions considered. Activity of each chemical in the reaction quotient is

substituted by the same value as the actual molar concentration of the chemical in the present reaction system, and specifically, both activities of H_2 and NH_3, which cannot be determined exactly, are substituted by 10^{-6} to obtain referential values. As shown in Table 2, all the redox potentials shift to the negative direction with increasing both pH and temperature, which can result in a negative shift of the mixed potential. Even the redox potentials of reactions 3 and 4 shift to the negative direction with increasing pH; the former is normally constant with pH and the latter increases with the increase in pH at a constant activity of Cu(II) ions. This is because the equilibrium activity of Cu^{2+} aquo ion decreases with increasing pH under the coexistence of abundant solid CuO in equilibrium, which brings about the negative shift of the redox potentials of reactions 3 and 4. Thus, possibly the mixed potential is shifted to the negative direction with increasing pH and temperature because the redox potentials of all the partial reactions shift to the negative direction. Consequently, factors to change the mixed potential are pH and temperature, which are easily controllable.

4. Experimental confirmation

Is it actually possible to control oxidation state of nanoparticles by controlling the mixed potential? This query was substantiated through the following experimental procedure.

4.1 Procedure

Reaction solutions were prepared using cupric oxide (CuO) (Kanto Chemical, Inc.), sodium hydroxide (NaOH), hydrazine monohydrate ($N_2H_4 \cdot H_2O$) (Nacalai Tesque, Inc.), and gelatin (Jellice Co. Ltd., P459) as received. All chemicals except for gelatin were of reagent grade. Gelatin was added as a dispersing agent to avoid agglomeration and for the suppression of particle growth. Gelatin blocked oxygen and was also effective in preventing the oxidation of the resulted nanoparticles. Reactions were conducted in a Pyrex beaker 250 cm^3 in capacity by the following procedure. First, a CuO colloidal aqueous suspension was prepared by dispersing 0.060 moles of CuO particles in 42.0 cm^3 of distilled water using ultrasound. Next, 18.0 cm^3 of 10 wt % gelatin aqueous solution was added into the solution as a dispersing agent. The initial pH of the mixed solution was adjusted to the reaction pH (9.0–12.0) at 298 K by 1.0 mol dm^{-3} sodium hydroxide aqueous solution with a pH meter (Horiba, Ltd., D-21). The temperature of the solution was kept at the reaction temperature (298–353 K) in a water bath with nitrogen gas bubbling (50 cm^3 min^{-1}), which started 30 min before the reaction and lasted throughout the reaction to eliminate the effect of dissolved oxygen. The solution was agitated at a rate of 500 rpm with a magnetic stirring unit. Then, 42.0 cm^3 of 1.43 mol dm^{-3} hydrazine aqueous solution was added to 18.0 cm^3 of 10 wt % gelatin aqueous solution, and this solution was kept at the reaction temperature (298–353 K) with nitrogen gas bubbling (50 cm^3 min^{-1}) for 30 min. The initial pH of the hydrazine solution was adjusted to the reaction pH (9.0–12.0) by 1.0 mol dm^{-3} sodium hydroxide aqueous solution at 298 K. Next, the hydrazine solution was added to the CuO aqueous suspension as a reducing agent to start the reaction. The total amount of the reaction suspension was 120.0 cm^3, and thus the reaction suspension was 0.50 mol dm^{-3} hydrazine aqueous solution with 0.50 mol dm^{-3} dispersed CuO. Gelatin was not added in the reaction suspension at 298 K because gelatin became a gel at 298 K, inhibiting the reaction. The crystalline structure of precipitates was investigated by X-ray diffraction (XRD: MAC Science Co., Ltd., M03XHF22) using a molybdenum X-ray tube. The morphology of precipitates was observed using a field-emission scanning electron microscope (JEOL Ltd., JSM-6500F). The immersion potential of Au-sputtered round quartz-crystal substrates 5.0 mm

diameter was measured during several experimental runs by a potentiostat/ galvanostat (Hokuto Denko Co., Ltd., HA-151), and it was assumed that the measured immersion potential was almost the same as the mixed potential in reaction suspension in this system. A Ag/AgCl electrode (Horiba, Ltd., 2565A-10T) was used as a reference electrode, and the internal liquid, 3.33 mol dm^{-3} KCl aqueous solution, was replaced for each experimental run. The measured potential was converted to values vs. SHE using the following empirical equation given by Horiba, Ltd. The potential of the reference electrode could be expressed as a function of temperature T (K) as E (mV) vs. SHE = +206 − 0.7(T − 298).

4.2 Results

In the present method, pH of the reaction suspension is initially adjusted at 298 K, and actual pH at reaction temperatures differs from the adjusted value. This is ascribable to the change in the ionic product for water, K_w = [H$^+$][OH$^-$]; for example, the value of K_w (mol^2 dm^{-6}) is 1.008 x 10^{-14} at 298.15 K and 5.476 x 10^{-14} at 323.15 K. Figure 4 shows the change with temperature in pH, which is initially adjusted to 9.0 at 298 K. pH linearly decreases with increasing temperature, and the values are 9.0 at 298 K, 8.5 at 323 K, and 7.6 at 353 K. Figure 5 shows the change in the mixed potential during the reaction for 2 h. At the same temperature of 323 K, the mixed potential at pH 10.4 (Fig. 5d) is lower than that at pH 8.5 (Fig. 5b). This agrees well with the discussion in the previous theory section.
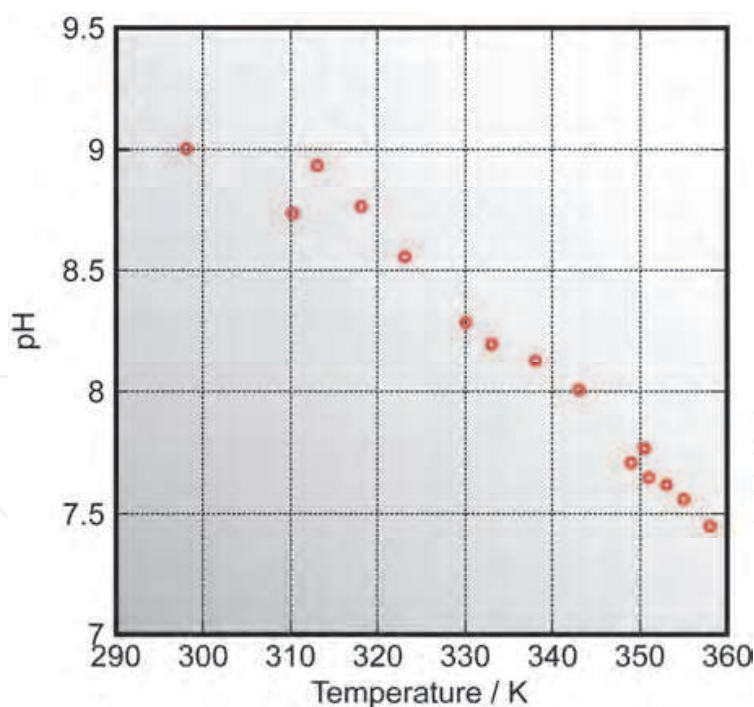

Fig. 4. Change in pH of the reaction suspension with temperature; pH of the reaction suspension was initially adjusted to 9.0 at 298 K.
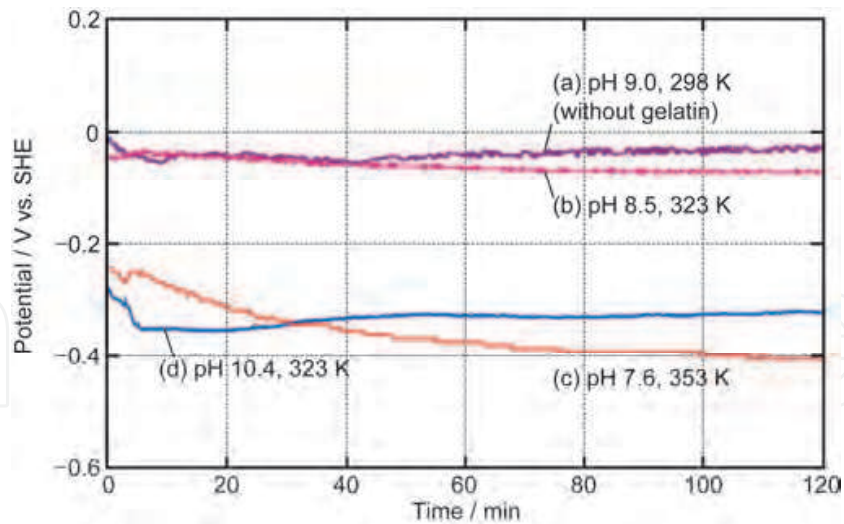
Fig. 5. Mixed potentials measured during the reaction at (a) pH 9.0, 298 K (without gelatin), (b) pH 8.5, 323 K, (c) pH 7.6, 353 K, and (d) pH 10.4, 323 K.
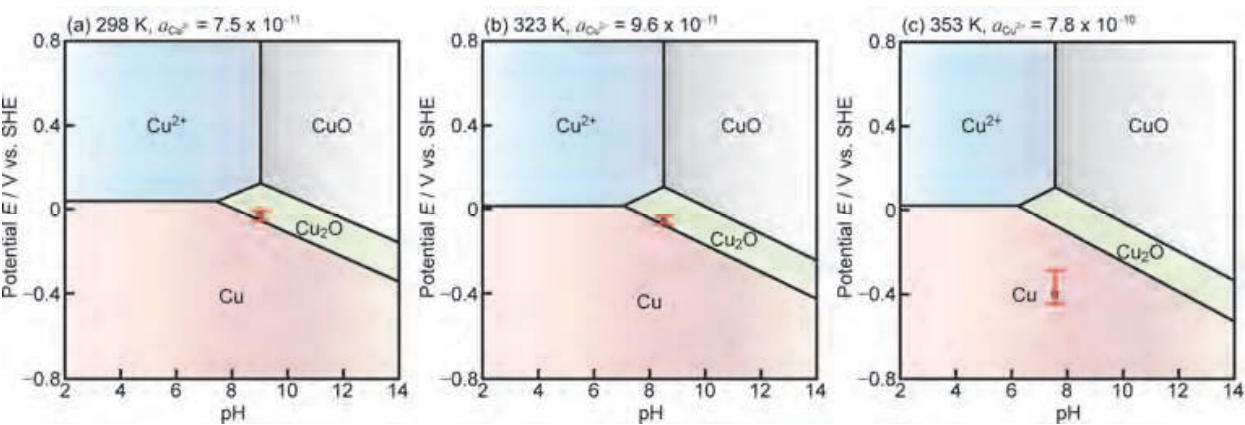

Fig. 6. Potential–pH diagrams drawn at the equilibrium activities of Cu^{2+} aquo ion at (a) pH 9.0, 298 K, (b) pH 8.5, 323 K, and (c) pH 7.6, 353 K considering the species Cu^{2+}, CuO, Cu_2O, and Cu. Bars and circles indicate the range and average value of the measured mixed potential, respectively.
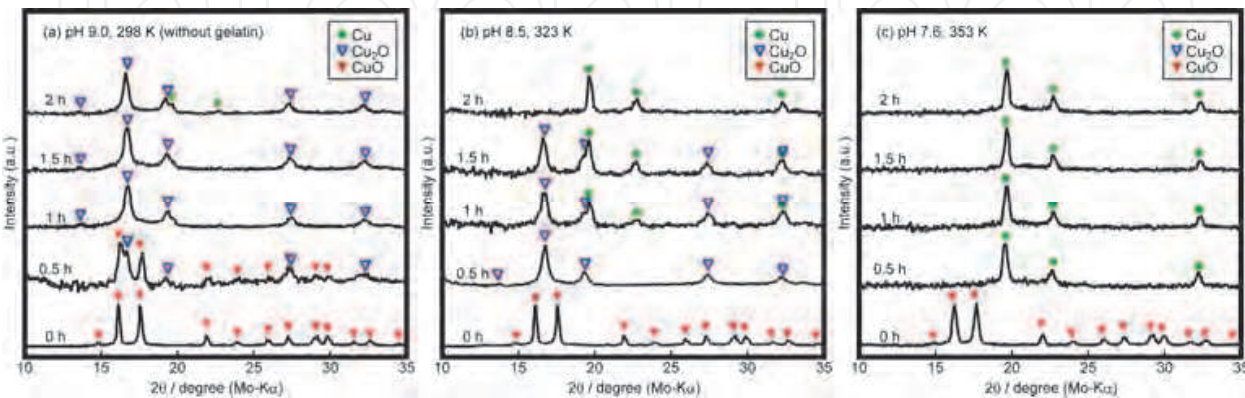

Fig. 7. XRD patterns of precipitates obtained during the reaction at (a) pH 9.0, 298 K (without gelatin), (b) pH 8.5, 323 K, and (c) pH 7.6, 353 K for 2 h.

Moreover, the mixed potential shifts to the negative direction with increasing temperature although pH slightly decreases, indicating that the mixed potential can be lowered just by increasing temperature without fixing pH. By comparing the mixed potential and the potential–pH diagrams shown in Fig. 6, the mixed potential was in the stability region of Cu_2O both at pH 9.0, 298 K (Fig. 6a) and pH 8.5, 323 K (Fig. 6b), whereas the mixed potential was in the stability region of metal Cu at pH 7.6, 353 K (Fig. 6c). Figure 7 shows the change with time in XRD patterns of precipitates during the reaction for 2 h. CuO powder was reduced to Cu_2O after 1 h at pH 9.0, 298 K although slight Cu peaks are recognized in the XRD pattern taken at 2 h. At pH 7.6, 353 K, CuO powder was completely reduced to metal Cu after 0.5 h. These results are almost consistent with the result that the mixed potentials measured at pH 7.6, 353 K and pH 9.0, 298 K were always in the stability region of Cu and Cu_2O, respectively. In contrast, at pH 8.5, 323 K, all CuO powder was reduced to Cu_2O after 0.5 h and then the resulting Cu_2O was gradually reduced to Cu metal. This is not consistent with the measurement result of the mixed potential. By carefully observing the change in the mixed potential at pH 8.5, 323 K, the initial mixed potential is −0.045 V vs. SHE and in the stability region of Cu_2O, and the mixed potential gradually decreases to −0.072 V with reaction time, which is just beside the calculated redox potential of Cu_2O/Cu, −0.077 V vs. SHE; i.e., as CuO is reduced to Cu_2O, the mixed potential approaches the redox potential of Cu_2O/Cu redox pair, where Cu_2O and Cu coexist. Nevertheless, the mixed potential is 5 mV higher than the calculated redox potential of Cu_2O/Cu and it is difficult to adequately elaborate on the result that the deposition of Cu completely proceeded after 2 h. Here, pH of the solution tends to slightly decrease during the reaction, although ideally, pH would not be changed by taking into account the overall reaction in the present reaction system. For example, pH actually decreased from 8.5 to approximately 8 at 323 K, resulting in a slight increase in the redox potential of a Cu_2O/Cu redox pair. The extra pH change is caused by the decrease in the equilibrium concentration of protonated hydrazine $N_2H_5^+$ due to the decrease in the total amount of hydrazine species by decomposition or oxidization during the reaction. Furthermore, there can be a slight difference between the mixed potential measured using Au electrode and the actual mixed potential in the reaction suspension. Therefore, the actual mixed potential is slightly lower than the redox potential of the Cu_2O/Cu redox pair. Nonetheless, a Au electrode is preferable for the measurement of the mixed potential in this reaction system because a Au electrode does not have intense catalytic activity for a specific partial reaction possible in the reaction system, and the effect of the immersion of the Au substrate is extremely low (Iacovangelo, 1991; Iacovangelo & Zarnoch, 1991).

The scanning electron microscopy (SEM) images of the precipitates obtained by the reaction are shown in Fig. 8. Relatively large Cu_2O particles with an average diameter of 475 nm are observed in the precipitates obtained after 2 h at pH 9.0, 298 K. These large particles are attributable to the absence of a dispersing agent, gelatin. At pH 8.5, 323 K, Cu_2O particles with an average diameter of 97 nm are observed after 0.5 h and Cu particles with an average diameter of 82 nm are observed after 2 h. Cu particles with an average diameter of 55 nm are observed after 2 h at 353 K. As above, the mean particle size is decreased with the increase in temperature because nucleation site increases with the increase in temperature and an inordinate number of nucleation sites at high temperatures leads to the absence of reactant ions (Cu(II) or Cu(I) ions) for the growth.

(a) pH 9.0, 298 K, 2h (Without gelatin)   (b) pH 8.5, 323 K, 2h

500 nm   500 nm

(c) pH 7.6, 353 K, 2h   (d) pH 8.5, 323 K, 0.5 h

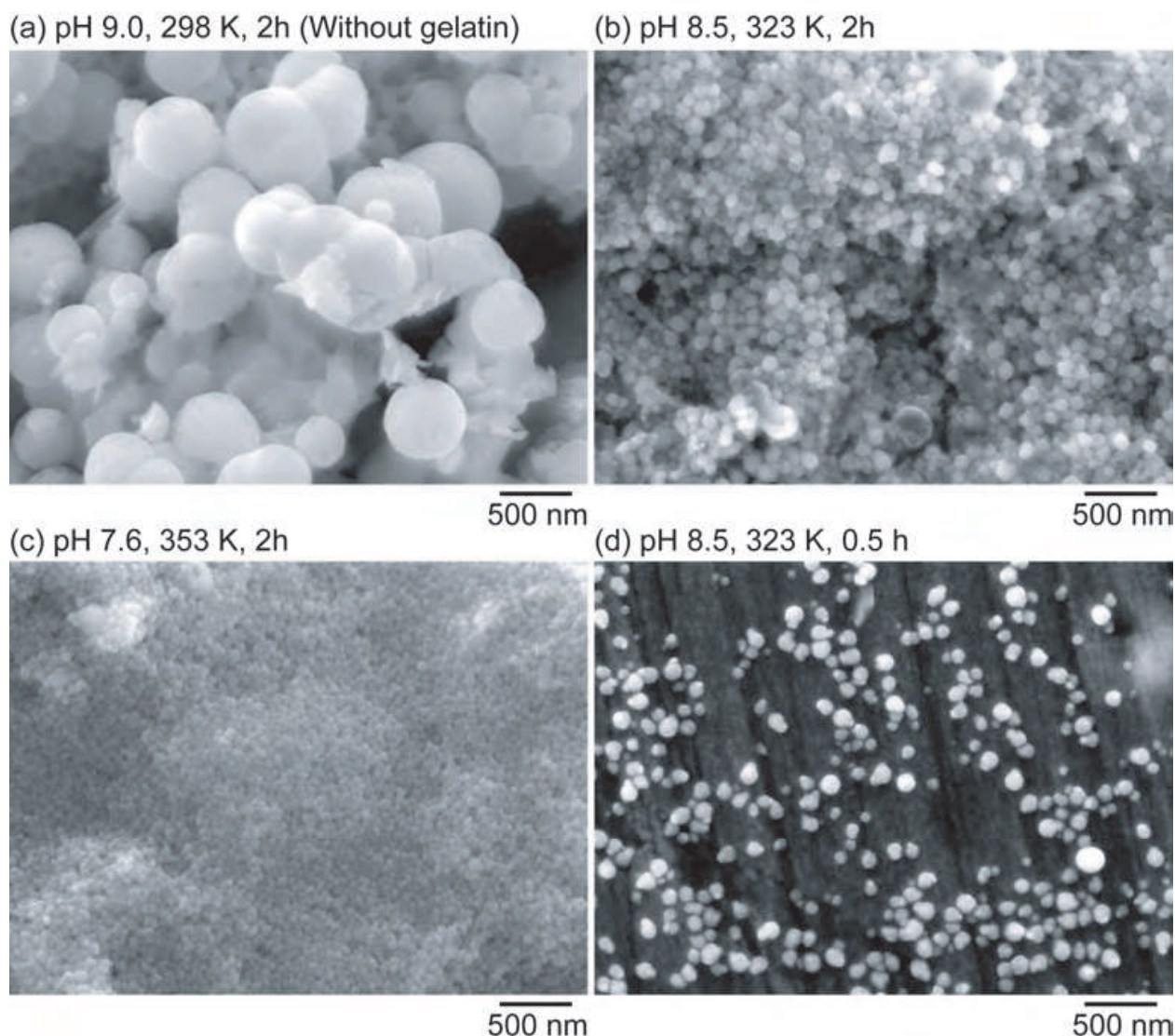500 nm   500 nm

Fig. 8. SEM images of precipitates obtained by the reaction at (a) pH 9.0, 298 K (without gelatin), (b) pH 8.5, 323 K, (c) pH 7.6, 353 K for 2 h, and (d) pH 8.5, 323 K for 0.5 h.

5. Conclusions

Mixed potential is the most effective indicator of solution circumstances, indicating the most stable chemical species in the reaction solution, i.e., thermodynamic considerations in conjunction with monitoring of mixed potential is useful for the in situ prediction of "what chemical species will be synthesized." Solution pH and temperature are the factors which affect the mixed potential, and thus, the most stable chemical species can be changed by pH and temperature. Specifically in this system, the mixed potential decreases with the increase both in pH and temperature. Using this concept, the selective synthesis of Cu and Cu_2O nanoparticles was demonstrated. This concept is also effective in other reaction systems where thermodynamic data are available. Furthermore in another journal (Yagi et al, 2010), the authors also reported that this concept can be widely applied and helps us to thermodynamically consider even those systems where insufficient or no thermodynamic data are available by experimentally measuring the redox potential with voltammetry combined with quartz crystal microbalance.

6. Acknowledgment

7. References

Beverskog B. & Puigdomenech I. (1997), Revised Pourbaix Diagrams for Copper at 25 to 300°C, *Journal of the Electrochemical Society*, Vol.144, No. 10, pp.3476-3483, ISSN 0013-4651

Bockris, J. O'M; Reddy, A. K. N. & Gamboa-Aldeco, M. (2000). *Modern Electrochemistry 2A: Fundamentals of Electrodics* (2nd ed.), Kluwer Academic/Plenum Publishers, ISBN 0-306-46167-6, New York, USA.

Cheng, Z.; Xu, J, Zhong, H., Chu, X.Z., & Song J. (2011). Repeatable Synthesis of Cu_2O Nanorods by a Simple and Novel Reduction Route, *Materials Letters*, Vol.65, pp.1871-1874, ISSN 0167-577X

Criss, C. M. & Cobble, J. W. (1964), The Thermodynamic Properties of High Temperature Aqueous Solutions. IV. Entropies of the Ions up to 200° and the Correspondence Principle, *Journal of the American Chemical Society*, Vol.86, pp.5385-5393, ISSN 0002-7863

Dhas, N. A.; Raj, C. P. & Gedanken, A. (1998). Synthesis, Characterization, and Properties of Metallic Copper Nanoparticles, *Chemistry of Materials*, Vol.10, pp.1446-1452, ISSN 0897-4756

Gou, L. & Murphy, C. J. (2003). Solution-Phase Synthesis of Cu_2O Nanocubes, *Nano Letters*, Vol.3, No.2, pp.231-234, ISSN 1530-6984

Gu, Y.-E; Zhang, Y., Zhang, F., Wei, J., Wang, C., Du, Y., & Ye, W. (2010). Investigation of Photoelectrocatalytic Activity of Cu_2O Nanoparticles for p-Nitrophenol using Rotating Ring-Disk Electrode and Application for Electrocatalytic Determination, *Electrochimica Acta*, Vol.56, pp.953-958, ISSN 0013-4686

Han, W. K.; Choi, K. W., Hwang, G. H., Hong, S. J., Lee, J. S., & Kang, S. G. (2006). Fabrication of Cu Nano Particles by Direct Electrochemical Reduction from CuO Nano Particles, *Applied Surface Science*, Vol.252, pp.2832-2838, ISSN 0169-4332

Huang, H. H.; Yan, F. Q., Kek, Y. M., Chew, C. H., Xu, G. Q., Ji, W., Oh, P. S., & Tang, S. H. (1997). Synthesis, Characterization, and Nonlinear Optical Properties of Copper Nanoparticles, *Langmuir*, Vol.13, pp.172-175, ISSN 0743-7463

Huang, L.; Jiang, H., Zhang, J., Zhang, Z., & Zhang, P. (2006). Synthesis of Copper Nanoparticles Containing Diamond-Like Carbon Films by Electrochemical Method, *Electrochemistry Communications*, Vol.8, pp.262-266, ISSN 1388-2481

Iacovangelo, C. D. & Zarnoch, K. P. (1991). Substrate-Catalyzed Electroless Gold Plating, *Journal of the Electrochemical Society*, Vol.138, No.4, pp.983-988, ISSN 0013-4651

Iacovangelo, C. D. (1991). Autocatalytic Electroless Gold Deposition Using Hydrazine and Dimethylamine Borane as Reducing Agents, *Journal of the Electrochemical Society*, Vol.138, No. 4, pp.976-982, ISSN 0013-4651

Joshi, S. S.; Patil, S. F., Iyer, V., & Mahumuni, S. (1998). Radiation Induced Synthesis and Characterization of Copper Nanoparticles, *Nanostructured Materials*, Vol.10, No.7, pp.1135-1144, ISSN 0965-9773

Kubaschewski, O. & Alcock, C. B. (1979), *Metallurgical Thermochemistry* (5th ed. Revised and enlarged), Elsevier, ISBN 0-08-022107-6, New York, USA

Kumar, R. V.; Mastai, Y., Diamant, Y., & Gedanken, A. (2001). Sonochemical Synthesis of Amorphous Cu and Nanocrystalline Cu_2O Embedded in a Polyaniline Matrix, *Journal of Materials Chemistry*, Vol.11, pp.1209-1213, ISSN 0959-9428

Latimer, W. M. (1959), *The Oxidation States of the Elements and Their Potentials in Aqueous Solutions* (2nd ed.), Prentice-Hall, Englewood Cliffs, New Jersey, USA.

Li J.; Liu, C.-Y. & Xie, Z. (2011). Synthesis and Surface Plasmon Resonance Properties of Carbon-coated Cu and Co Nanoparticles, *Materials Research Bulletin*, Vol.46, pp.743-747, ISSN 0025-5408

Lisiecki, I. & Pileni, M. P. (1993). Synthesis of Copper Metallic Clusters Using Reverse Micelles as Microreactors, *Journal of the American Chemical Society*, Vol.115, pp.3887-3896, ISSN 0002-7863

Lisiecki, I.; Billoudet, F. & Pileni, M. P. (1996). Control of the Shape and the Size of Copper Metallic Particles, *Journal of Physical Chemistry*, Vol.100, pp.4160-4166, ISSN 0022-3654

Liu, R.; Oba, F., Bohannan, E. W., Ernst, F., & Switzer, J. A. (2003). Shape Control in Epitaxial Electrodeposition: Cu_2O Nanocubes on InP(001), *Chemistry of Materials*, Vol.15, pp.4882-4885, ISSN 0897-4756

Liu, X.; Geng, B., Du, Q., Ma, J., & Liu, X. (2007). Temperature-Controlled Self-Assembled Synthesis of CuO, Cu_2O and Cu Nanoparticles Through a Single-Precursor Route, *Materials Science and Engineering: A*, Vol.448, pp.7-14, ISSN 0921-5093

Lu, C.; Qi, L., Yang, J., Wang, X., Zhang, D., Xie, J., & Ma, J. (2005). One-Pot Synthesis of Octahedral Cu_2O Nanocages via a Catalytic Solution Route, *Advanced Materials*, Vol.17, pp.2562-2567, ISSN 1521-4095

Mahajan, M.B.; Pavan, M.S. & Joy, P.A. (2009). Ferromagnetic Properties of Glucose Coated Cu_2O Nanoparticles, *Solid State Communications*, Vol.149, pp.2199-2201, ISSN 0038-1098

Muramatsu, A. & Sugimoto T. (1997). Synthesis of Uniform Spherical Cu_2O Particles from Condensed CuO Suspensions, *Journal of Colloid and Interface Science*, Vol.189, pp.167-173, ISSN 0021-9797

Ohde H.; Hunt, F. & Wai, C. M. (2001). Synthesis of Silver and Copper Nanoparticles in a Water-in-Supercritical-Carbon Dioxide Microemulsion, *Chemistry of Materials*, Vol.13, pp.4130-4135, ISSN 0897-4756

Potential-pH Diagrams for
Oxidation-State Control of Nanoparticles Synthesized via Chemical Reduction
239

Pileni, M. P. & Lisiecki, I., (1993). Nanometer Metallic Copper Particle Synthesis in Reverse Micelles, *Colloids and Surfaces A: Physicochemical and Engineering Aspects,* Vol.80, pp.63-68, ISSN 0927-7757

Poizot, P.; Laruelle, S., Grugeon, S., Dupont, L., & Tarascon, J-M. (2000). Nano-sizedtransition-metaloxidesas negative-electrode materials for lithium-ion batteries, *NATURE*, Vol. 407, pp.496-499, ISSN 0028-0836

Pourbaix, M. (1974). *Atlas of Electrochemical Equilibria in Aqueous Solutions* (2nd ed.), NACE International, Cebelcor, Brüssel, Belgium

Qi, L.; Ma, J. & Shen J. (1997). Synthesis of Copper Nanoparticles in Nonionic Water-in-Oil Microemulsions, *Journal of Colloid and Interface Science*, Vol.186, pp.498-500, ISSN 0021-9797

Singh, M.; Sinhaa, I., Premkumarc, M., Singhc, A.K., & Mandal, R.K. (2010). Structural and Surface Plasmon Behavior of Cu Nanoparticles using Different Stabilizers, *Colloids and Surfaces A: Physicochemical and Engineering Aspects*, Vol.359, pp.88-94, ISSN 0927-7757

Siwach, O. P. & Sen, P., (2010). Study of fluorescence properties of Cu nanoparticles, *Solid State Sciences,* Vol.12, pp.1107-1111, ISSN 1293-2558

Snoke D. (2002). Spontaneous Bose Coherence of Excitons and Polaritons, *Science*, Vol.298, pp.1368-1372, ISSN 0036-8075

Stull, D. R. & Prophet, H. (1971), *JANAF Thermochemical Tables* (2nd ed.), NSRDS-NBS, Washington, DC, USA

Wang, W.; Wang, G., Wang, X., Zhan, Y., Liu, Y., & Zheng, C. (2002). Synthesis and Characterization of Cu_2O Nanowires by a Novel Reduction Route, *Advanced Materials*, Vol.14, No. 1, pp.67-69, ISSN 1521-4095

Yagi, S.; Nakanishi, H., Ichitsubo, T. & Matsubara, E. (2009). Oxidation-State Control of Nanoparticles Synthesized via Chemical Reduction Using Potential Diagrams, *Journal of the Electrochemical Society*, Vol.156, No.8, pp.D321-D325, ISSN 0013-4651

Yagi, S.; Kawamori, M. & Matsubara, E. (2010). Electrochemical Study on the Synthesis Process of Co–Ni Alloy Nanoparticles via Electroless Deposition, *Journal of the Electrochemical Society*, Vol.157, No.5, pp.E92-E97, ISSN 0013-4651

Yeh, M.-S.; Yang, Y.-S., Lee, Y.-P., Lee, H.-F., Yeh, Y.-H., & Yeh, C.-S. (1999). Formation and Characteristics of Cu Colloids from CuO Powder by Laser Irradiation in 2-Propanol, *The Journal of Physical Chemistry B*, Vol.103, pp.6851-6857, ISSN 1089-5647

Young, A. P. & Schwartz, C. M. (1969). Electrical Conductivity and Thermoelectric Power of Cu_2O, *Journal of Physics and Chemistry of Solids*, Vol.30, pp.249-252, ISSN 0022-3697

Yu, L.; Sun, H., He, J., Wang, D., Jin, X., Hu, X., & Chen, G. Z. (2007). Electro-reduction of Cuprous Chloride Powder to Copper Nanoparticles in an Ionic Liquid, *Electrochemistry Communications*, Vol.9, pp.1374-1381, ISSN 1388-2481

Zhang, C.Q.; Tu, J.P., Huang, X.H., Yuan, Y.F., Chen, X.T., & Mao F. (2007). Preparation and Electrochemical Performances of Cubic Shape Cu_2O as Anode Material for Lithium Ion Batteries, *Journal of Alloys and Compounds*, Vol.441, pp.52–56, ISSN 0925-8388

Zhang, J.; Liu, J., Peng, Q., Wang, X., & Li, Y. (2006). Nearly Monodisperse Cu_2O and CuO Nanospheres: Preparation and Applications for Sensitive Gas Sensors, *Chemistry of Materials*, Vol.18, pp.867-871, ISSN 0897-4756

Zhang, X.D.; Xi, J.F., Shen, Y.Y., Zhang, L.H., Zhu, F., Wang, Z., Xue, Y.H. & Liu, C.L. (2011).
        Thermal Evolution and Optical Properties of Cu Nanoparticles in SiO₂ by Ion
        Implantation, *Optical Materials*, Vol.33, pp.570-575, ISSN 0925-3467
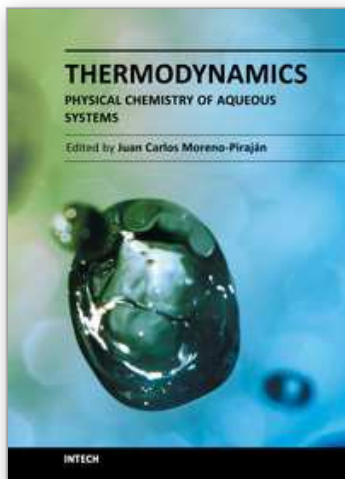
Thermodynamics - Physical Chemistry of Aqueous Systems

Edited by Dr. Juan Carlos Moreno Pirają́n

Thermodynamics is one of the most exciting branches of physical chemistry which has greatly contributed to the modern science. Being concentrated on a wide range of applications of thermodynamics, this book gathers a series of contributions by the finest scientists in the world, gathered in an orderly manner. It can be used in post-graduate courses for students and as a reference book, as it is written in a language pleasing to the reader. It can also serve as a reference material for researchers to whom the thermodynamics is one of the area of interest.

How to reference

In order to correctly reference this scholarly work, feel free to copy and paste the following:

Shunsuke Yagi (2011). Potential-pH Diagrams for Oxidation-State Control of Nanoparticles Synthesized via Chemical Reduction, Thermodynamics - Physical Chemistry of Aqueous Systems, Dr. Juan Carlos Moreno Pirają́n (Ed.), ISBN: 978-953-307-979-0, InTech, Available from:
http://www.intechopen.com/books/thermodynamics-physical-chemistry-of-aqueous-systems/potential-ph-diagrams-for-oxidation-state-control-of-nanoparticles-synthesized-via-chemical-reductio

INTECH
open science | open minds